Advances in Nano Research, *Vol. 19, No. 4 (2025) 383-397*
https://doi.org/10.12989/anr.2025.19.4.383

Analytical solution of transient temperature distribution in curved beam

Ashkan Nourizadeh Dehkordi, Mohammad Arefi*, Mohsen Irani Rahaghi and E. Mohammad-Rezaei Bidgoli

Department of Solid Mechanic, Faculty of Mechanical Engineering, University of Kashan, Kashan, Iran

(*Received February 11, 2025, Revised August 22, 2025, Accepted September 29, 2025*)

Abstract. In this study, analytical solution of transient temperature distribution of curved beam is presented for various boundary conditions. After derivation of the governing equation, solution for temperature distribution in curved beam is derived using an exact analytical method. The results are obtained for three different boundary conditions. The solution is obtained using separation of variables method. Applying the various boundary conditions yields unknown constants in terms of input parameters. The accuracy and trueness of the obtained solution and corresponding numerical results are satisfied using comparison with available results of literature. The results are presented for various types of the thermal boundary conditions.
Keywords: analytical solution; curved beam; transient temperature distribution; various boundary conditions

1. Introduction

Curved structures can be used in the various mechanical elements and systems specially in the aerospace science and civil engineering. The analysis of these types of the structures and systems is a requirement for advanced structural analysis. The multi-field loading especially thermal loading has significant impact on the responses of the curved structures. Because of this important effect, in this paper, the thermal analysis of the curved beams is presented.

Haskul (2019) studied the stress analysis of cylindrically curved functionally graded material (FGM) beams under radial thermal loading. Material properties, except for Poisson's ratio, varied radially according to a power law. Analytical methods were used to examine stresses and displacements under various temperature gradients, applying the von Mises yield criterion to determine elastic limits. Arefi and Zenkour (2017) investigated thermal stress and deformation analysis of size-dependent curved nanobeams using sinusoidal shear deformation theory. Governing equations were derived based on nonlocal thermoelasticity, analyzing the effects of thermal loads, nonlocal elasticity, foundation stiffness, and curvature radius on displacements and stresses. Arefi and Zenkour (2017) conducted electro-magneto-elastic bending and free vibration analysis of a sandwich curved beam with an elastic core and piezo-magnetic face sheets. They derived governing equations using first-order shear deformation theory and investigated the influence of Pasternak's foundation parameters, electric, and magnetic potentials on displacement, stress, and natural frequencies. Arefi and Zenkour (2017) studied the electro-magneto-elastic behavior of a three-layer curved beam with piezo-magnetic face sheets. Using first-order shear deformation theory, they analyzed bending and vibration under the influence of electric and magnetic potentials and Pasternak's foundation, highlighting the effects on deflection and vibration characteristics.

Beg and Yasin (2021) examined the bending, free, and forced vibration of functionally graded deep curved beams in a thermal environment using an efficient layerwise theory. Equations of motion were derived through the Hamiltonian approach, incorporating the rule of mixture and Mori–Tanaka scheme for material homogenization. Analytical solutions were developed using Fourier series for simply supported boundary conditions. Pandey and Pradyumna (2021) studied transient thermal stresses in functionally graded sandwich curved beams subjected to thermal shock using a higher-order layerwise theory. Finite element formulations were developed based on Hamilton's principle, and the effects of geometric and material parameters on thermal stresses were investigated. Sayyad and Avhad (2022) conducted thermal analysis of laminated composite, sandwich, and functionally graded curved beams using a fifth-order curved beam theory. They accounted for transverse shear and normal strains, deriving analytical solutions using Navier's method for simply supported curved beams under thermal loads. Boğa and Selek (2020) investigated axial stress analysis of functionally graded beams under thermal loading using both analytical and numerical methods. Different FGM configurations with material properties varying according to a power law along the thickness were analyzed, and results were validated using ANSYS finite element simulations. Arefi (2015) analyzed stress distribution in curved beams made of FGMs under pure bending using linear elasticity theory. Analytical expressions for radial and circumferential stress distributions were derived for various cross-sectional shapes, examining the effects of positive and negative nonhomogeneity indices.

Mohammadi and Dryden (2008) developed an analytical solution for thermal stress in functionally graded curved beams under uniform temperature changes. The study

*Corresponding author, Professor,
E-mail: arefi63@gmail.com; arefi@kashanu.ac.ir

ISSN: 2287-237X (Print), 2287-2388 (Online)

examined radial variations of elastic stiffness and compared stress fields between FGM-coated and solid rings.

Yousefi and Rastgoo (2011) conducted free vibration analysis of functionally graded spatial curved beams using first-order shear deformation theory (FSDT). They applied the Ritz method to determine natural frequencies and analyzed the effects of curvature, boundary conditions, and helix pitch angle on dynamic behavior. Yapıcı *et al*. (2008) studied transient temperature and thermal stress distributions in a stationary hollow steel disk heated by a moving uniform heat source. They developed a numerical model using finite volume and finite difference methods, demonstrating the influence of thermal conductivity, angular speed, and heated segment area on thermal stresses. Yapıcı and Başẗurk (2005) analyzed transient temperature and thermally induced stress distributions in a solid steel disk under radially periodic heating using a finite volume-based computational fluid dynamics (CFD) approach. Effects of thermal conductivity, heat flux speed, and periodic heating were explored to mitigate stress-induced damage. Sadooghi (2005) examined transient heat transfer in spherical protective materials exposed to flux and mixed boundary conditions. An analytical solution incorporating radiation and conduction heat transfer was developed, demonstrating the importance of material properties for thermal protection. Araya and Gutierrez (2006) derived analytical solutions for transient three-dimensional temperature distribution in finite solids due to a moving laser beam. They compared spatially uniform and Gaussian heat source models, emphasizing the impact of boundary effects on temperature distribution. Jiang and Dai (2015) investigated steady and transient heat conduction in double-layer plates with functionally graded materials (FGM). Analytical solutions were developed using the Poisson method and separation of variables, exploring the effects of material properties, heat source location, and geometric parameters. Forced vibration analysis of the composite beam was studied by Civalek *et al* (2021). Sobhani *et al* (2022) studied the impact of agglomeration on the vibration analysis of curved shells and structures. Uzun *et al* (2020) studied the impact of various boundary conditions and elastic foundation on the vibration responses of the beam. Hadji *et al* (2021) presented an analytical solution for free vibration analysis of the nanoplates. Civalek and Demir (2011) presented the nonlocal continuum model for buckling and static bending analyses of carbon nanotube beams.

Malekzadeh *et al*. (2012) studied transient response of rotating laminated functionally graded cylindrical shells under thermal environments using differential quadrature and Newmark's time integration methods. The study examined dynamic responses based on temperature-dependent material properties and boundary conditions. Ootao and Ishihara (2013) developed a three-dimensional analytical solution for transient thermoelastic response of functionally graded rectangular plates under non-uniform heat supply. The effects of material gradation and heat distribution on stress fields were analyzed. Boo and Cho (1990) investigated transient temperature distributions in finite-thickness plates during arc welding using an analytical solution to the heat conduction equation. The model was validated through experiments on steel plates, demonstrating its application for feedback control and process optimization.

Tahani *et al*. (2010) analyzed transient responses of functionally graded hollow circular cylinders under dynamic loads using finite element and Newmark methods. Dynamic wave characteristics were explored, highlighting the advantages of FGMs in enhancing stress distribution and stability. Yang *et al*. (2019) studied transient heat conduction in coated steel plates with two-layer coatings using a combination of Fourier and non-Fourier methods. Boundary conditions and coating parameters were examined for optimizing transient temperature fields. Qian *et al*. (2022) developed analytical solutions for temperature distribution in laminated beams under general thermal boundary conditions. The effects of beam thickness, material properties, and layer configuration on thermal fields were investigated. Amiri Delouei *et al*. (2020) derived a two-dimensional analytical solution for steady-state heat conduction in thick hollow spheres made of FGMs. The study validated results through test cases and explored the influence of conductivity ratios on temperature distribution.

Wu *et al*. (2019) investigated transient heat conduction in multilayered slabs under various boundary conditions using superposition and separation of variables methods. Applications in landfill thermal analysis were demonstrated.

Jin and Paulino (2001) analyzed transient thermal stress around an edge crack in FGM strips. They used a layered material model and Laplace transform to calculate thermal stress intensity factors, emphasizing design considerations under thermal shock conditions. Eslami *et al*. (2005) examined thermal and mechanical stresses in thick hollow spheres made of FGMs. Analytical solutions for temperature, displacement, and stress components were derived, demonstrating the optimization potential of material gradation. Azzara *et al*. (2023) analyzed vibration and buckling of isotropic and composite beams under thermal loads using the Carrera Unified Formulation (CUF). The study provided benchmark solutions and explored the influence of lamination and geometry on thermal instability.

Zhang *et al*. (2023a) studied transient thermoelastic behavior of rectangular plates under time-dependent convection and radiation boundaries. They validated their analytical method against finite element simulations, highlighting the impact of boundary conditions on displacement and stress. Abouelregal and Alesemi (2022) examined thermal and mechanical behavior of fiber-reinforced magnetic viscoelastic solids using the Moore-Gibson-Thompson (MGT) thermoelastic model. Analytical and numerical solutions were developed to explore the effects of viscosity, reinforcement, and thermal pulses on structural responses.

Tang *et al*. (2023) derived analytical solutions for thermal buckling of rotationally restrained orthotropic thin plates with non-classical boundary conditions. Critical temperatures and mode shapes were calculated, demonstrating excellent agreement with finite element results. Aljadani and Zenkour (2022) studied thermal shock response of

rotating infinite media using generalized thermoelastic models. Effects of rotation and decay parameters on temperature, displacement, and stress fields were graphically illustrated. Yang *et al*. (2020) analyzed nonlinear vibration of functionally graded carbon nanotube-reinforced composite beams with temperature-dependent properties. Higher-order shear deformation theory was used to derive motion equations, exploring thermal and geometric nonlinearity effects. Ansari *et al*. (2022) examined nonlinear thermally induced vibrations of porous functionally graded Timoshenko beams embedded in elastic media. Hamilton's principle and the Newmark algorithm were applied to study the influence of porosity, boundary conditions, and geometric properties. Zhou *et al*. (2020) derived analytical formulas for temperature-induced deformation in long-span suspension bridges. The study validated models using field data from the Tsing Ma Bridge, emphasizing the dominant role of cable temperature in structural deformation. Tran *et al*. (2022) investigated nonlinear vibration of porous FGM sandwich plates under blast loading using Reddy's higher-order shear deformation theory. Parametric studies demonstrated the impact of material and loading conditions on vibration behavior.

The analysis of micro- and nano-scale structures has become a cornerstone of modern engineering, driven by the development of advanced materials like functionally graded composites, graphene-based reinforcements, and smart materials with piezoelectric and piezomagnetic properties. Accurately predicting the mechanical behavior of these complex structures—such as shells, plates, and sandwich panels—requires sophisticated theoretical frameworks that extend beyond classical continuum mechanics. At small scales, size-dependent effects become significant, necessitating the application of nonlocal elasticity and modified couple stress theories (MCST) to capture the nuanced interplay between material microstructure and macroscopic response. Furthermore, the interaction of these structures with their environment, including elastic foundations and multi-physical fields (e.g., electro-elastic and magneto-electro-elastic environments), adds another layer of complexity to their analysis. Substantial research has been dedicated to this field, as evidenced by extensive studies on the bending, vibration, and static response of various geometries. Investigations have covered the electro-elastic analysis of piezoelectric doubly curved shells on elastic foundations (Arefi and Bidgoli 2019) and the nonlocal free vibration of piezoelectric nano-shells (Arefi 2018). The magneto-electro-mechanical bending of exponentially graded microplates (Arefi and Kiani 2020) and the influence of magneto-electric environments on nanobeams (Arefi and Zenkour, 2019) further highlight the critical role of multi-physical coupling. Recent advancements have incorporated novel materials like graphene origami, with studies examining their reinforcement of doubly curved shells (Yang *et al*. 2023a) and their use in sandwich cylindrical panels (Vali and Arefi 2023). The vibrational behavior of complex systems, including truncated conical porous sandwich micro/nano-shells reinforced with graphene platelets (Adab and Arefi 2022) and sandwich microshells analyzed with dynamic formulations that consider thickness-stretching (Zhang *et al*. 2023b), has also been a key area of focus. These analyses often employ higher-order shear deformation theories to account for through-thickness effects accurately, as seen in the bending response of functionally graded composite doubly curved nanoshells (Arefi *et al*. 2022) and the static analysis of shells on elastic foundations using nonlocal elasticity (Arefi and Civalek 2020). Collectively, this body of work demonstrates a consistent effort to refine theoretical models for the precise mechanical characterization of advanced micro- and nano-structures under multi-field conditions.

The contemporary engineering landscape is characterized by a synergistic advancement across multiple disciplines, where innovations in materials, manufacturing, digitalization, and environmental science are deeply interconnected. This progress is fundamentally driven by the development of advanced materials and composites, which form the backbone of modern infrastructure and technology. Research spans from enhancing the performance of traditional materials, such as investigating the flexural behavior of corroded steel beams (Tang *et al*. 2025) and improving cement-based materials with carbon nanotubes (Yang and Zhu 2023), to pioneering new multi-functional composites. Notable examples include carbon fiber composites enhanced with MXene and CNT nanomaterials (Shang *et al*. 2025), analytical models for corrugated rolling of composite plates (Liu *et al*. 2025a). A diverse range of cellulose and chitosan-based biocomposites for applications from optical management films to environmental remediation (Chen *et al*. 2025c, Xu *et al*. 2018, Xiong *et al*. 2023, Zhang *et al*. 2025) was investigated in the literature.

Parallel to material innovations, a revolution in digital and intelligent manufacturing is underway, leveraging sophisticated computational methods to achieve unprecedented precision and control. This is exemplified by digital-twin-enabled systems for real-time monitoring of tube wrinkling (Wang *et al*. 2025a), advanced registration algorithms for 3D bent tubes (Wang *et al*. 2025b), and edge-deployable frameworks for thermal error compensation in machining (Liu *et al*. 2025b). The efficacy of these digital tools is often validated by cutting-edge experimental and monitoring techniques, such as Ultraviolet Stereo-Digital Image Correlation for extreme-temperature deformation measurement (Luo *et al*. 2024).

Understanding and managing thermal and multiphysical phenomena is another critical frontier, with research addressing challenges from the micro-scale to the geophysical. Studies focus on highly efficient thermal management for spindle systems using grooved heat pipes and topology optimization (Ma *et al*. 2025a, b). The thermal-mechanical properties of geothermal reservoirs (Wu *et al*. 2025), and the development of granular thermodynamic frameworks to model complex multiphase flow, solute transport, and crystallization in soils (Bai *et al*. 2025a, b, c) were studied in the literature. These thermodynamic principles find further application in dynamic systems, such as devices for vibration control and energy harvesting (Zou *et al*. 2021) and the analysis of vehicle dynamics and wheel-rail creep behavior in metro systems (Chen *et al*. 2025a, b).

Underpinning these experimental and applied efforts are robust computational and analytical methodologies. These range from meshless symplectic algorithms for solving nonlinear wave equations (Zhang *et al*. 2017) and solvers for time-domain integral methods (Zhang *et al*. 2012) to the application of novel materials like egg-white/titania composites for photocatalytic degradation (Feng *et al*. 2020). A significant and unifying theme across these disciplines is the focus on sustainability and environmental protection. This is evidenced by the extensive development of eco-friendly adsorbents—such as porous bamboo carbon and plasma-modified nanofibers for gaseous formaldehyde capture (Su *et al*. 2023, Xiong *et al*. 2024)—and advanced filtration membranes for removing heavy metals from water (Xiong *et al*. 2023, Zhang *et al*. 2025), collectively highlighting the engineering community's commitment to addressing pressing environmental challenges.

The literature review was presented in the Introduction section. The paper is studied the analytical solution for thermal analysis of curved beam subjected to various thermal boundary conditions. The thermal conductivity equation is solved using the analytical method for various boundary conditions. The solution method is confirmed through comparison with available results in the literature. The complete results are presented along the radial and circumferential directions for various boundary conditions.

2. Formulation

The aim of this study is to present a transient analytical solution for temperature distribution of a curved beam. In this paper, the method of separation of variable is used for solving the heat equation. The transient thermal conductivity equation in cylindrical coordinate system is presented as follows (Sayyad and Avhad 2022, Andey and Pradyumna 2021, Mohammadi and Dryden 2008):

$$\rho C_p \frac{\partial \tau}{\partial t} = k[\frac{\partial^2 \tau}{\partial^2 r} + \frac{1}{r}\frac{\partial \tau}{\partial r} + \frac{1}{r^2}\frac{\partial \tau}{\partial^2 \theta}] \quad (1)$$

The schematic figure of the curved beam is presented in Fig.1

In Eq. (1), ρ is density, C_p is specific heat capacity and k is thermal conductivity coefficient. The governing equation should be solved for a schematic curved presented in Fig.1. The curved beam has inner and out radii ri and ro, respectively. For solving the Eq. (1) in this study, the separation of variable used.

The boundary condition of the curved beam is included isolated condition at inner radius and heat flux at outer radii. Furthermore, the initial temperature is assumed T_0.

The solution of the governing equations is strongly depending on the type of boundary conditions. For this study three types of boundary conditions are assumed named as type A, type B and type C. out radii ri and ro, respectively. For solving the equation (1) in this study, the separation of variable used.

The boundary condition of the curved beam is included isolated condition at inner radii and heat flux at outer radii. Furthermore, the initial temperature is assumed T_0.

The solution of the governing equations is strongly depending on the type of boundary conditions. For this study three types of boundary conditions are assumed named as type A, type B and type C.

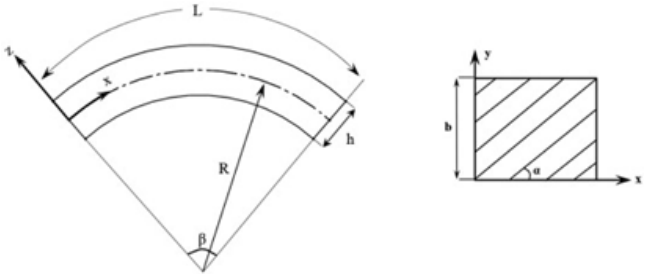

Fig. 1 The schematic figure of a curved beam subjected to transient thermal loading

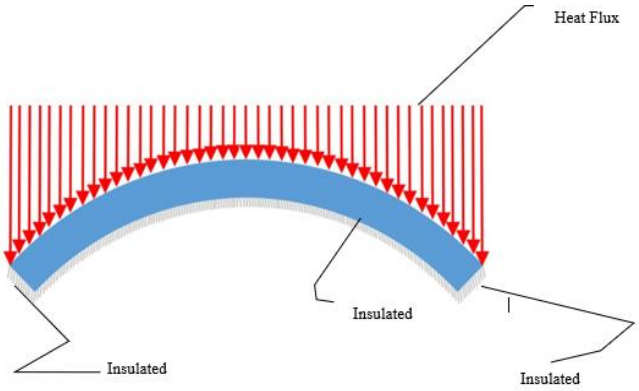

Fig. 2 Curved Beam with Boundary condition type A

2.1 Boundary condition type A

Fig. 2 shows the schematic figure of type A boundary condition. This type of boundary condition is included a heat flux exposed to outer radius and isolated condition for outer surfaces.

The boundary conditions for type A are mathematically expressed as follows:

$$B.C \;\; type\; A \rightarrow \begin{cases} \frac{\partial \tau}{\partial r}_{r=ri} = 0 \\ \frac{\partial \tau}{\partial r}_{r=ro} = f(\theta)\cos(\omega t) \quad and \;\; \omega = cte \\ \frac{\partial \tau(r.\theta_a.t)}{\partial \theta} = \frac{\partial \tau(r.\theta_b.t)}{\partial \theta} = 0 \end{cases} \quad (2)$$

Based on the method of separating the variables, the general

$$\tau = R(r)T(t)\Theta(\theta) \quad (3)$$

Solution of the temperature equation is considered as:
Substitution of Eq. (3) into Eq. (1) yields:

$$\frac{\dot{T}}{T} = k\left[\frac{\ddot{R}}{R} + \frac{\dot{R}}{rR} + \frac{\ddot{\Theta}}{r^2\Theta}\right] \quad (4)$$

With considering $\frac{1}{k} = a^2$, the governing equation is simplified as:

$$\frac{\ddot{R}}{R} + \frac{\dot{R}}{rR} + \frac{\ddot{\Theta}}{r^2\Theta} = \frac{a^2\dot{T}}{T} = \mu_1 \quad (5)$$

Some manipulation on the Eq. (5) yields:

$$\frac{a^2\,\acute{T}}{T} = \mu_1 \implies a^2\,\acute{T} - \mu_1 T = 0 \Rightarrow \acute{T} - \frac{\mu_1}{a^2}T = 0 \quad (6)$$

With considering $-\frac{\mu_1}{a^2} = i\omega$, Eq. 6 is solved as:

$$T(t) = e^{i\omega t} = \cos\omega t + i\sin\omega t \;.\; and\; \mu_1 = a^2 i\,\omega \quad (7)$$

Therefore, the temperature distribution $\tau(r.\theta.t)$ is derived as follows (Sayyad and Avhad 2022, Andey and Pradyumna 2021, Mohammadi and Dryden 2008):

$$\tau(r.\theta.t) = Re\{\tau(r.\theta)e^{i\omega t}\} \quad (8)$$

To find $\Theta(\theta)$, we also use separation of variables as:

$$r^2\frac{\ddot{R}}{R} + r\frac{\dot{R}}{R} - r^2\mu_1 = r^2\frac{\ddot{R}}{R} + r\frac{\dot{R}}{R} - r^2a^2 i\,\omega = -\frac{\ddot{\Theta}}{\Theta} = \mu_2 \quad (9)$$

With considering $\mu_2 = n^2$, the unknown function is derived as:

$$\Theta(\theta) = A_n\cos n\theta + B_n\sin n\theta \quad n = 1.2.3.\ldots\ldots \quad (10)$$

By applying the Boundary condition proposed in Eq. 2, the Eq. 10 become as:

$$\begin{aligned}&\frac{\partial\tau(r.\theta_a = 0.t)}{\partial\theta} = \frac{\partial\tau(r.\theta_b.t)}{\partial\theta} = 0\\ &\Rightarrow -A_n\sin(n\theta) + B_n\cos(n\theta) = 0\\ &\Rightarrow A_n\cos(n\theta) = 0 \Rightarrow B_n = 0\end{aligned} \quad (11)$$

Finaly $\Theta(\theta)$ is obtained as follows:

$$\Theta(\theta) = A_n\cos n\theta \quad (12)$$

Using Eq. 12, the differential equation of $R(r)$ is rearranged as follows:

$$\begin{aligned}&r^2\frac{\ddot{R}}{R} + r\frac{\dot{R}}{R} - r^2a^2 i\,\omega - n^2 \Rightarrow\\ &r^2\ddot{R} + r\dot{R} - (ia^2\omega\, r^2 + n^2)R = 0\end{aligned} \quad (13)$$

Solution of $R(r)$ using the Kelvin Differential equation is derived as:

$$\begin{aligned}R = {} & C_n\left[ber_n\left(a\sqrt{\omega}\,r\right) + ibei_n\left(a\sqrt{\omega}\,r\right)\right]\\ & + D_n\left[ker_n\left(a\sqrt{\omega}\,r\right) + ikei_n\left(a\sqrt{\omega}\,r\right)\right]\end{aligned} \quad (14)$$

The temperature distribution is now obtained as follows:

$$\begin{aligned}\tau = R(r)T(t)\Theta(\theta) = \tau(r.\theta.t) = {} & \Big(\sum_{n=0}^{\infty} C_n\left[ber_n\left(a\sqrt{\omega}\,r\right) + ibei_n\left(a\sqrt{\omega}\,r\right)\right]\\ & + D_n\left[ker_n\left(a\sqrt{\omega}\,r\right)\right.\\ & \left. + ikei_n\left(a\sqrt{\omega}\,r\right)\right]\Big) \times A_n\cos n\theta\\ & \times e^{i\omega t}\end{aligned} \quad (15)$$

And finally transient temperature distribution will be obtained as:

$$\tau(r.\theta.t) =$$

$$\begin{aligned}&\Big(\sum_{n=0}^{\infty} H_n\left[ber_n\left(a\sqrt{\omega}\,r\right) + ibei_n\left(a\sqrt{\omega}\,r\right)\right] \quad (16)\\ &+\left[ker_n\left(a\sqrt{\omega}\,r\right) + ikei_n\left(a\sqrt{\omega}\,r\right)\right]\Big) \times \acute{A}_n\cos n\theta \times e^{i\omega t}\end{aligned}$$

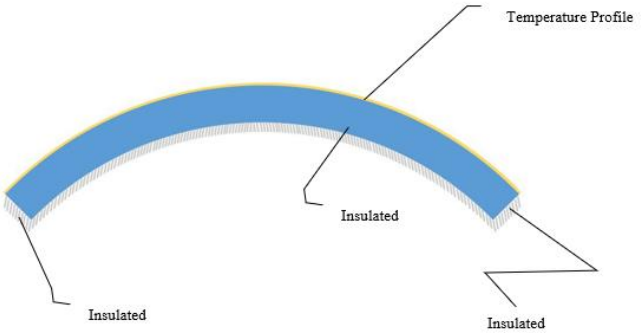

Fig. 3 Curved Beam with Boundary condition type B

In which:

$$\begin{aligned}&P = \left[k\acute{e}r_n\left(a\sqrt{\omega}\,r_o\right) + ik\acute{e}\imath_n\left(a\sqrt{\omega}\,r_{r_o}\right)\right]\\ &Q = H_n \times \left[b\acute{e}r_n\left(a\sqrt{\omega}\,r_o\right) + ib\acute{e}\imath_n\left(a\sqrt{\omega}\,r_o\right)\right]\\ &\grave{A} = \frac{1}{\theta_b - \theta_a} \times \frac{1}{P+Q}\int_{\theta_a}^{\theta_b} f(\theta) \times \cos(n\theta)\,d\theta\end{aligned} \quad (17)$$

It is noted that the diagrams related to this boundary condition are presented in the results section.

2.2 Boundary condition type B

The boundary condition of type B is presented in Fig. 3, where three surfaces are insulated and other one is subjected to a temperature profile. Therefore, the boundary conditions in state B will be as follows:

$$B.C\ for\ typ\ B\text{:}\quad \begin{cases}\dfrac{\partial\tau}{\partial r}_{r=ri} = 0\\ \tau(ro.\theta.0) = f(\theta)\cos(\omega t) \quad and\ \ \omega = cte\\ \dfrac{\partial\tau(r.\theta_a.t)}{\partial\theta} = \dfrac{\partial\tau(r.\theta_b.t)}{\partial\theta} = 0\end{cases} \quad (18)$$

The temperature distribution is assumed as follows:

$$\tau = R(r)T(t)\Theta(\theta) \quad (19)$$

Using Eq. 22, the governing equation is simplified as follows:

$$\frac{\acute{T}}{T} = k\left[\frac{\ddot{R}}{R} + \frac{\dot{R}}{rR} + \frac{\ddot{\Theta}}{r^2\Theta}\right] \quad (20)$$

Using definition $\frac{1}{k} = a^2$, Eq. 20 is converted to:

$$\frac{\ddot{R}}{R} + \frac{\dot{R}}{rR} + \frac{\ddot{\Theta}}{r^2\Theta} = \frac{a^2\,\acute{T}}{T} = \mu_1 \quad (21)$$

Eq. 21 is converted to the unknown format to arrive the solution:

$$\frac{a^2\,\acute{T}}{T} = \mu_1 \implies a^2\,\acute{T} - \mu_1 T = 0 \Rightarrow \acute{T} - \frac{\mu_1}{a^2}T = 0 \quad (22)$$

Using definition $-\frac{\mu_1}{a^2} = i\omega$, the solution is derived as:

$$T(t) = e^{i\omega t} = \cos\omega t + i\sin\omega t \;.\; \mu_1 = a^2 i\,\omega \quad (23)$$

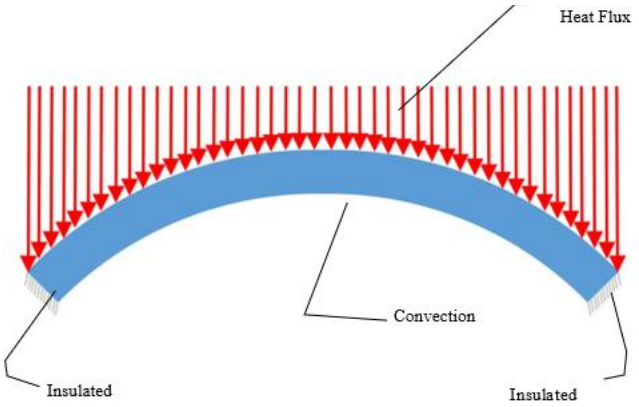

Fig. 4 Curved Beam with Boundary condition type C

Now, the solution for real part of $\tau(r.\theta.t)$ is obtained as (Sayyad and Avhad 2022, Andey and Pradyumna 2021, Mohammadi and Dryden 2008):

$$\tau(r.\theta.t) = Re\{\tau(r.\theta)e^{i\omega t}\} \tag{24}$$

For $\Theta(\theta)$ also by using separation of variables, we will have:

$$r^2\frac{\ddot{R}}{R} + r\frac{\dot{R}}{R} - r^2\mu_1 = r^2\frac{\ddot{R}}{R} + r\frac{\dot{R}}{R} - r^2a^2i\,\omega = -\frac{\ddot{\Theta}}{\Theta} = \mu_2 \tag{25}$$

Using definition $\mu_2 = n^2$, the solution of Eq. 25 is completed as:

$$\Theta(\theta) = A_n\cos n\theta + B_n\sin n\theta \quad n = 1.2.3.\ldots\ldots \tag{26}$$

Now by applying the boundary condition, we will have:

$$\frac{\partial\tau(r.\theta_a = 0.t)}{\partial\theta} = \frac{\partial\tau(r.\theta_b.t)}{\partial\theta} = 0 \Rightarrow B_n = 0 \tag{27}$$

And therefore the solution is obtained:

$$\Theta(\theta) = A_n\cos n\theta \tag{28}$$

Now the solution for $R(r)$ is obtained using Eq. 25 as:

$$r^2\frac{\ddot{R}}{R} + r\frac{\dot{R}}{R} - r^2a^2i\,\omega - n^2 \Rightarrow r^2\ddot{R} + r\dot{R} - (ia^2\omega\,r^2 + n^2)R = 0 \tag{29}$$

By applying the second Boundary condition relate to outer side on this curved beam,

$$\begin{aligned}&\tau(r.\theta.t)@t\;r = r_o = f(\theta)\cos(\omega t)\\ &f(\theta)\cos(\omega t) = (H_n\left[ber_n(a\sqrt{\omega}\,r_o) + ibei_n(a\sqrt{\omega}\,r_o)\right]\\ &+\left[ker_n(a\sqrt{\omega}\,r_o) + ikei_n(a\sqrt{\omega}\,r_o)\right])\\ &\times\acute{A}_n\cos n\theta\times e^{i\omega t} = f(\theta)\cos(\omega t)\end{aligned} \tag{30}$$

For calculation $\acute{A}_n$ used from Fourier transform

$$\begin{aligned}&X = \left[ker_n(a\sqrt{\omega}\,r) + ikei_n(a\sqrt{\omega}\,r)\right]\\ &S = H_n\times\left[ber_n(a\sqrt{\omega}\,r) + ibei_n(a\sqrt{\omega}\,r)\right]\\ &\grave{A} = \frac{1}{\theta_b-\theta_a}\times\frac{1}{[X+S\,]}\int_{\theta_a}^{\theta_b} f(\theta)\times\cos(n\theta)\,d\theta\end{aligned} \tag{31}$$

And finally transient temperature distribution will be as below:

$$\tau(r.\theta.t) = (\sum_{n=0}^{\infty} H_n\left[ber_n(a\sqrt{\omega}\,r) + ibei_n(a\sqrt{\omega}\,r)\right] + \left[ker_n(a\sqrt{\omega}\,r) + ikei_n(a\sqrt{\omega}\,r)\right]) \times\acute{A}_n\cos n\theta\times e^{i\omega t} \tag{32}$$

2.3 Boundary condition type C

As shown as in Fig. 4, in case C, the boundary conditions will be as follows. The outer radius is subjected to heat flux, the inner radius has convection with air, and the other two sides of the curved beam are insulated.

$$IC\rightarrow\{\tau(r.\theta.0) = T_0$$
$$\begin{cases}\dfrac{\partial\tau(r.\theta_a.t)}{\partial\theta} = \dfrac{\partial\tau(r.\theta_b.t)}{\partial\theta} = 0\\ \dfrac{\partial\tau}{\partial r}_{r=ro} = f(\theta)\cos(\omega t) \quad and\;\;\omega = cte\\ -k\dfrac{\partial\tau}{\partial r}_{r=r_i} = h\tau(r,\theta_a,t)\;\;bottom\;convection\;with\;air\end{cases} \tag{33}$$

And then the final answer of this temperature distribution is Real part of below relation:

$$\tau = (\sum_{n=0}^{\infty} C_n\left[ber_n(a\sqrt{\omega}\,r) + ibei_n(a\sqrt{\omega}\,r)\right] + D_n\left[ker_n(a\sqrt{\omega}\,r) + ikei_n(a\sqrt{\omega}\,r)\right]) \times A_n\cos n\theta\times e^{i\omega t} \tag{34}$$

Now, to find the coefficients of this equations, boundary condition should be apply on it. By applying the boundary conditions on Eq. (34)

At $r = r_i$ boundary condition is: $k\frac{\partial\tau(r.\theta.t)}{\partial T} = h\tau(r.\theta_a.t)$

$$\begin{aligned}&G = k(\left[b\acute{e}r_n(a\sqrt{\omega}\,r_i) + ib\acute{e}\imath_n(a\sqrt{\omega}\,r_i)\right])\\ &Z = h(\left[ber_n(a\sqrt{\omega}\,r) + ibei_n(a\sqrt{\omega}\,r)\right])\\ &K = k\left[k\acute{e}r_n(a\sqrt{\omega}\,r_i) + ik\acute{e}\imath_n(a\sqrt{\omega}\,r_i)\right]\\ &W = \left[ker_n(a\sqrt{\omega}\,r) + ikei_n(a\sqrt{\omega}\,r)\right]\\ &-\frac{G-Z}{K-W}\\ &= F_n\left[F_n\begin{bmatrix}b\acute{e}r_n(a\sqrt{\omega}\,r_o)\\ +ib\acute{e}\imath_n(a\sqrt{\omega}\,r_o)\end{bmatrix} + \begin{bmatrix}k\acute{e}r_n(a\sqrt{\omega}\,r_o)\\ +ik\acute{e}\imath_n(a\sqrt{\omega}r_o)\end{bmatrix}\right]D_nA_n\cos n\theta = \grave{A}\end{aligned} \tag{35}$$

the Eq. 32 becomes to below

$$\tau(r.\theta.t) = (\sum_{n=0}^{\infty} F_n\left[ber_n(a\sqrt{\omega}\,r) + ibei_n(a\sqrt{\omega}\,r)\right] + \left[ker_n(a\sqrt{\omega}\,r) + ikei_n(a\sqrt{\omega}\,r)\right])\acute{A}_n\cos n\theta\,e^{i\omega t} \tag{36}$$

Same above the second Boundary condition relate to outer side on this curved beam should be apply, finally, transient temperature distribution will be as below:

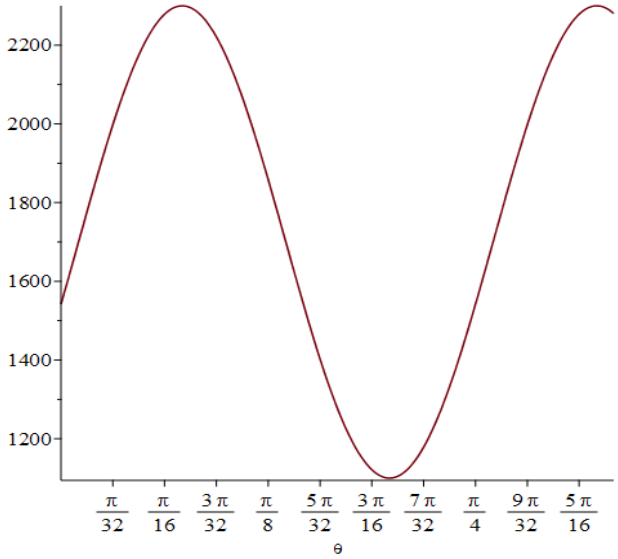

Fig. 5 Thermal flux distribution on the outer diameter of a curved beam

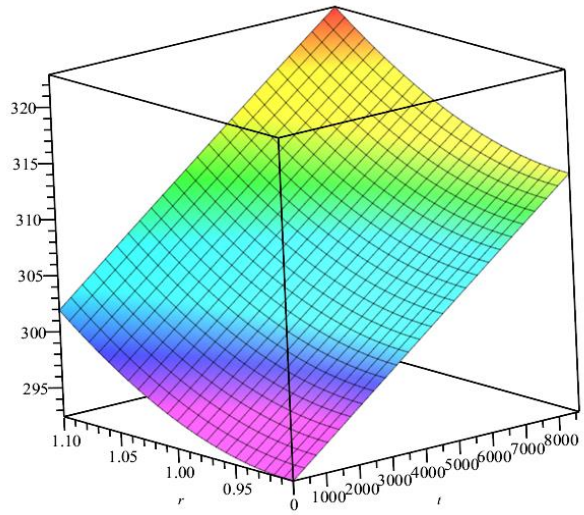

Fig. 6 3D temperature distribution along the radial direction

$$\tau(r.\theta.t) = (\sum_{n=0}^{\infty} H_n \left[ber_n(a\sqrt{\omega}\, r) + ibei_n(a\sqrt{\omega}\, r)\right] + \left[ker_n(a\sqrt{\omega}\, r) + ikei_n(a\sqrt{\omega}\, r)\right])\acute{A}_n \cos n\theta\, e^{i\omega t} \quad (37)$$

In which:

$$N = F_n\left[b\acute{e}r_n(a\sqrt{\omega}\, r_o) + ib\acute{e}\imath_n(a\sqrt{\omega}\, r_o)\right]$$
$$Y = \left[k\acute{e}r_n(a\sqrt{\omega}\, r_o) + ik\acute{e}\imath_n(a\sqrt{\omega}\, r_{r_o})\right] \quad (38)$$
$$\grave{A} = \frac{1}{\theta_b - \theta_a} \times \frac{1}{[\,N + Y\,]}$$

4. Result and validation

In this section, the analytical solution results for the curved beam under study were compared and validated against the numerical solution obtained through COMSOL simulations.

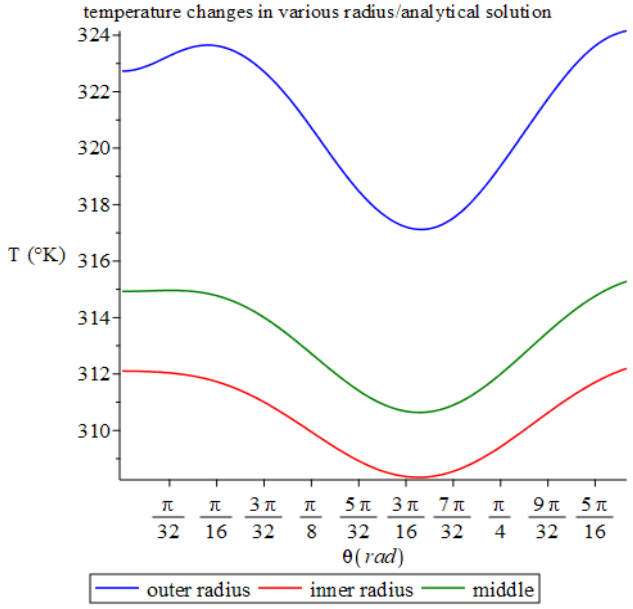

Fig. 7 Temperature distribution within a curved beam at the inner, middle, and outer radii

Evaluations were conducted under boundary conditions A, B, and C. Discussions on the agreement and discrepancies between the solutions were also included

4.1 Results and validation of boundary condition type A

4.1.1 Analytical solution results

For type A boundary conditions, Fig. 3 shows the distribution of the assumed heat flux applied to the outer radius. This graph represents the variation of heat flux applied along the angular direction (θ) on the outer radius of a curved beam. Fig. 5 shows the distribution of thermal flux applied to the outer diameter of a curved beam. The thermal flux is normalized by the maximum thermal flux and is plotted against the angle θ, which represents the position along the outer diameter of the curved beam. The relation of this heat flux is as equation No.38:

$$f(\theta) = 600 * sin(8 * \theta + 12.3) + 1700 \quad (39)$$

Therefore, the temperature distribution throughout the curved beam, based on the applied thermal flux under boundary condition type A, is described in the following section. The material properties are assumed as follows:

$$\rho = 8000\,kg/m^3, k = 17W/m^oK, C_p = 502\,J/kg^oK$$

Fig. 6 shows that the three-dimensional distribution of heat due to the assumed heat flux on the outer radius.

Fig. 7 shows temperature distribution within a curved beam under external heat flux. The graph illustrates the temperature variation as a function of the angular position (θ in radians) at the inner, middle, and outer radii of the beam. The analytical solution demonstrates distinct temperature profiles across the beam's radial sections, highlighting the influence of curvature on heat transfer.

Fig. 8 illustrates the three-dimensional temperature distribution across the inner, middle, and outer radii of the curved beam over time and angular position (θ). The results

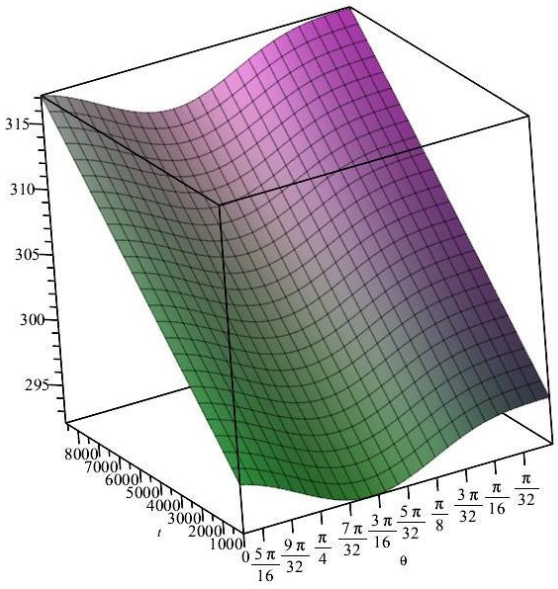

(a) Inner radius

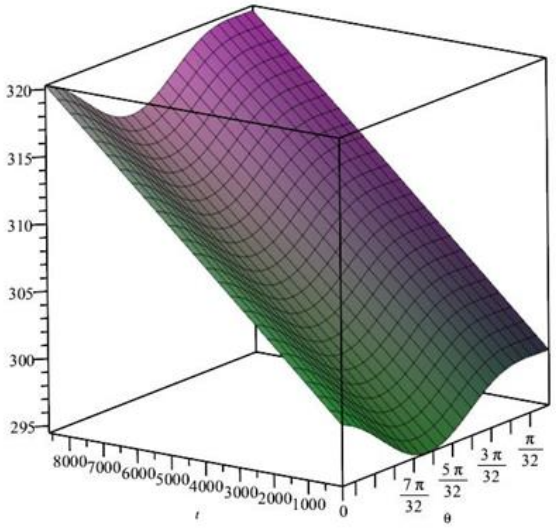

(b) Middle radius

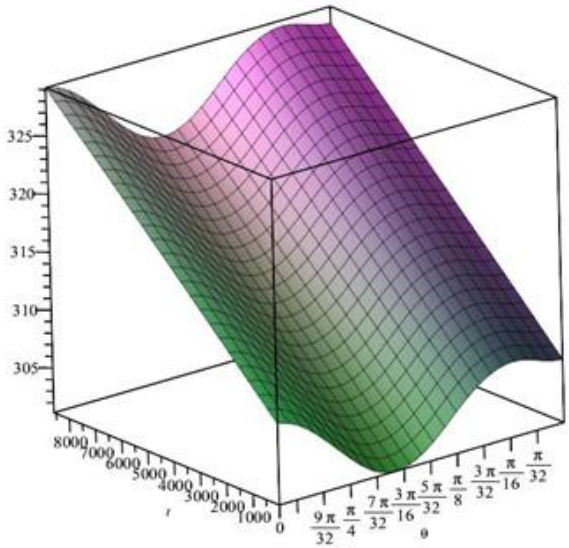

(c) Outer radius

Fig. 8 Three-dimensional temperature distribution in the curved beam with Boundary condition A

(a) In the beginning

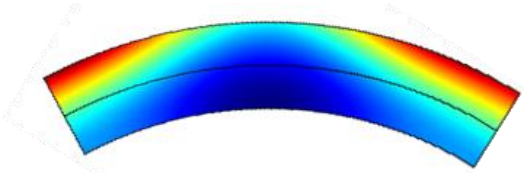

(b) At the end

Fig. 9 Temperature change a curved beam modeled by COMSOL with Boundary condition A

indicate that temperature decreases due to heat dissipation and exhibits periodic variations along θ, reflecting the non-uniform heat flux application. Over time, the temperature stabilizes as the system approaches thermal equilibrium, with peak values diminishing progressively across all radii.

4.1.2 Validation

This section presents a comparison between the analytical solution and the results obtained from COMSOL software simulations to evaluate their agreement.

The curved beam was modeled in COMSOL under boundary condition A. Fig. 9 illustrates the curved beam at the beginning and end of the time period during which it was subjected to the applied thermal flux.

Shown in Fig. 10 is the comparison between analytical and those results obtained from Comsol simulation along the circumferential direction. An acceptable agreement between the present theoretical and numerical results is observed.

As shown in Fig. 10, the results obtained from the analytical solution of the studied curved beam have been compared and evaluated with the solution provided by Comsol software.

4.2 Results and validation of boundary condition type B

4.2.1 Analytical solution results

Under boundary condition type B, the outer radius of the curved beam was subjected to a temperature profile. Fig. 11 presents the temperature profile applied to the outer radius of the curved beam. The corresponding thermal flux is defined by the equation provided in Eq. (40)

$$f(\theta) = (600 * sin(8\theta) + 1700) \quad (40)$$

Fig. 12 presents three-dimensional diagrams of the temperature distribution for boundary condition type B across the inner, middle, and outer radii of the curved beam. These diagrams illustrate the temperature variation over time (t) and angular position (θ). The surface plots highlight periodic temperature fluctuations along θ, which are influenced by the applied boundary conditions.

Fig. 13 shows Temperature distribution in the curved beam under Type B boundary conditions. The graph depicts

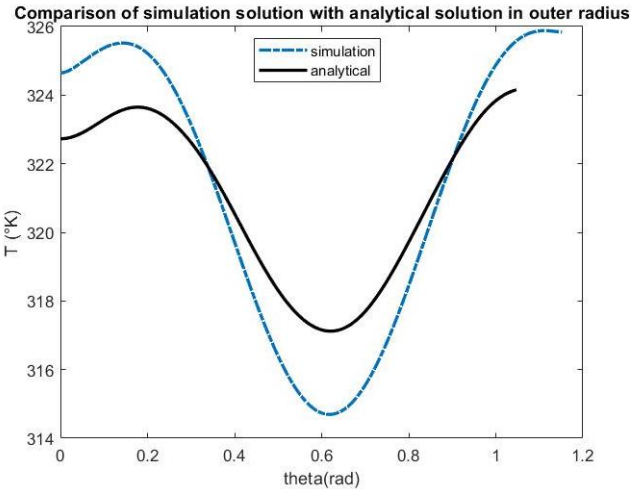

(a) Outre radius

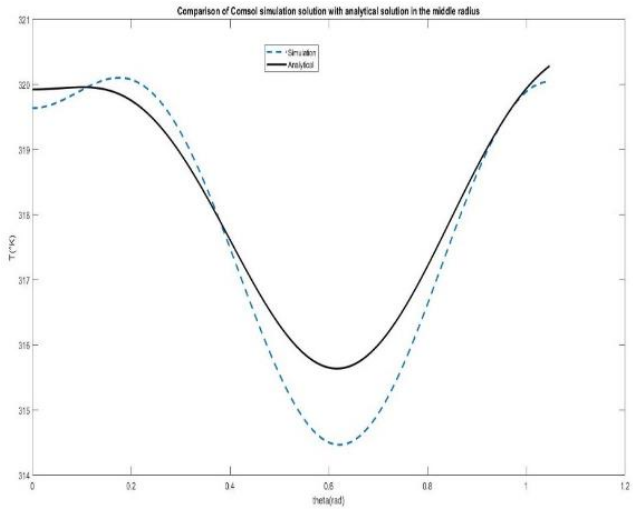

(b) Inner radius

Fig. 10 Comparison between analytical and those results obtained from Comsol simulation

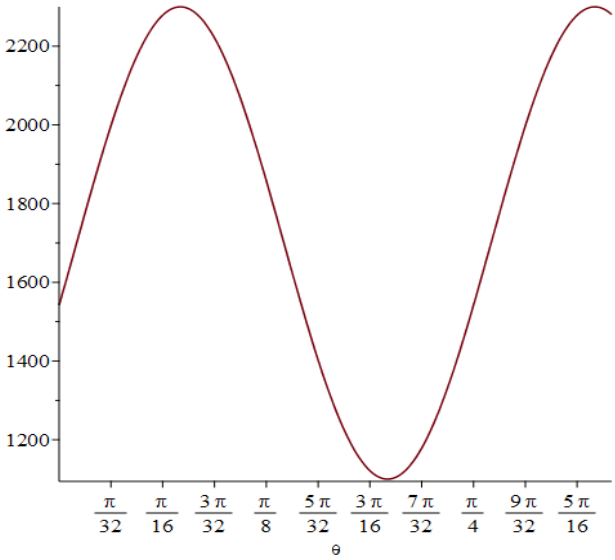

Fig. 11 Temperature Profile applied to outer radius in Boundary condition type B

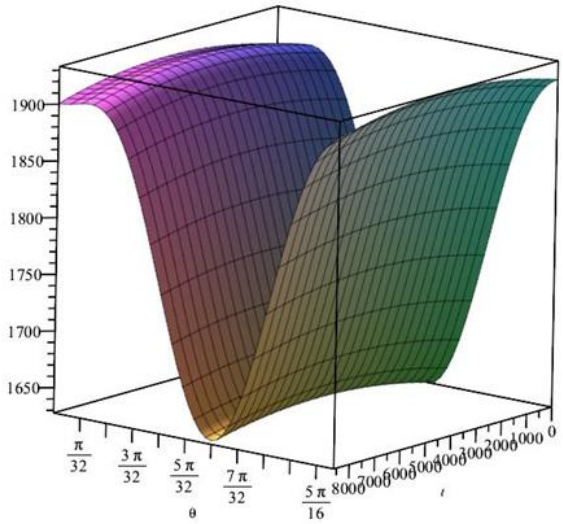

(a) Inner radius

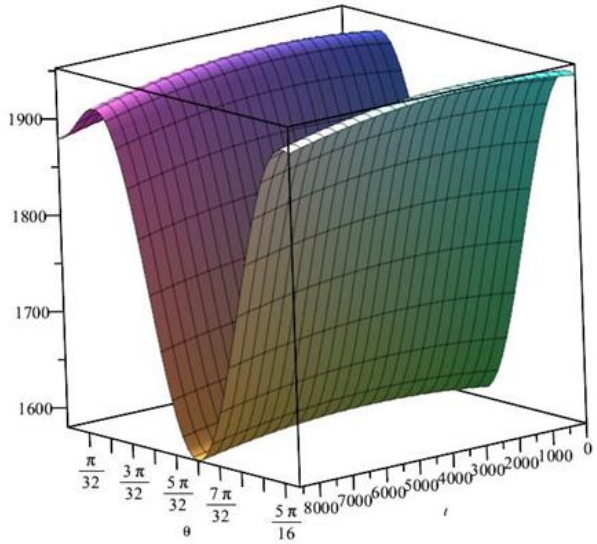

(b) Middle radius

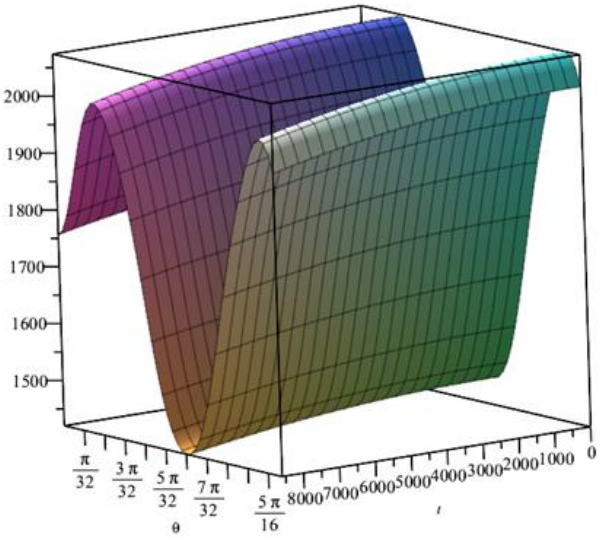

(c) Outer radius

Fig. 12 Three-dimensional temperature distribution in the curved beam with Boundary condition B

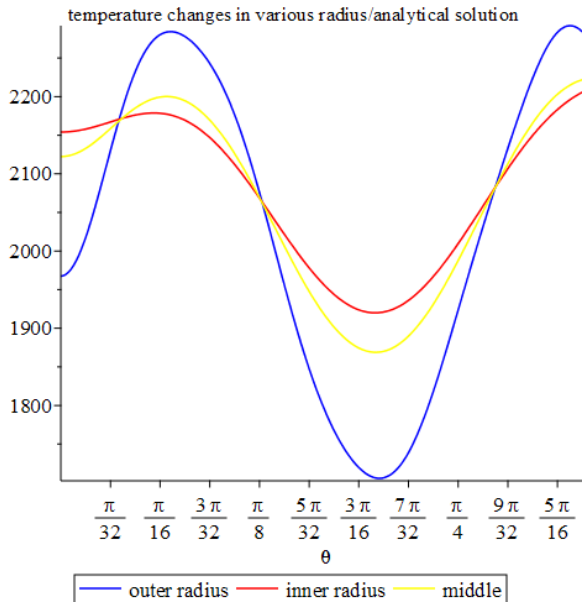

Fig. 13 2D temperature distribution in curved beam in Boundary condition type B

(a) In the beginning

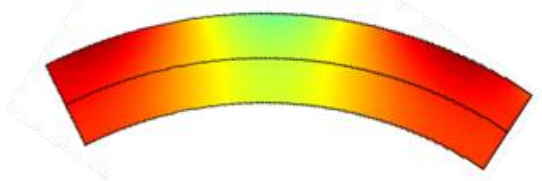

(b) At the end

Fig. 14 Temperature change a curved beam modeled by COMSOL with Boundary condition B

temperature variation as a function of angular position (θ, in radians) across the inner, middle, and outer radii of the beam. The results highlight the temperature profile within the curved beam, emphasizing the thermal response at different radial positions under the applied boundary conditions.

4.2.2 Validation

The curved beam was modeled in COMSOL under boundary condition B. Fig. 14 shows the curved beam at the beginning and end of the time period during which it was subjected to the applied thermal flux. The validation of the analytical solution against the COMSOL simulation results demonstrates a close agreement between the two, confirming the accuracy of the analytical solution.

For this case, the analytical solution was compared with the numerical solution obtained from COMSOL. The comparison charts are presented in Figs. 15(a) and (b), illustrating the temperature distribution along the circumferential direction of the curved beam. The analytical solution

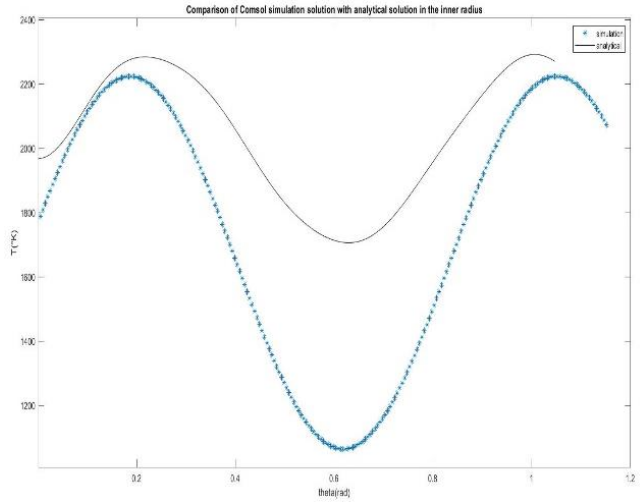

(a) Outre radius

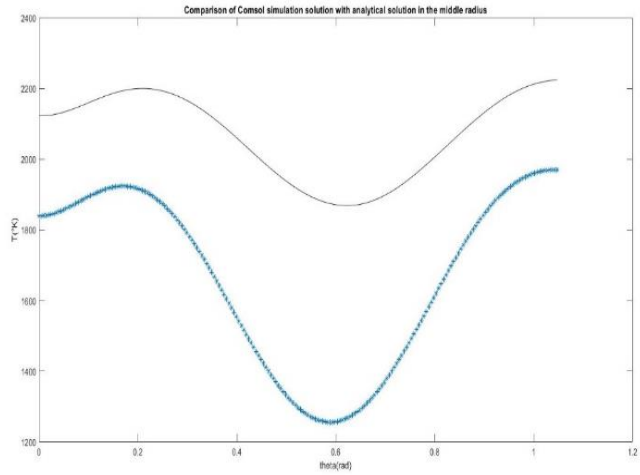

(b) Inner radius

Fig. 15 Comparison between analytical and those results obtained from Comsol simulation

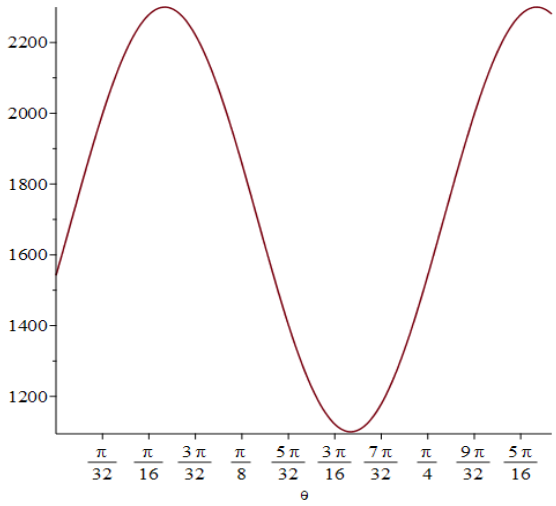

Fig. 16 Thermal flux applied to outer radius in Boundary condition type C

is represented by a solid gray line, while the COMSOL simulation results are shown as scattered blue points. The

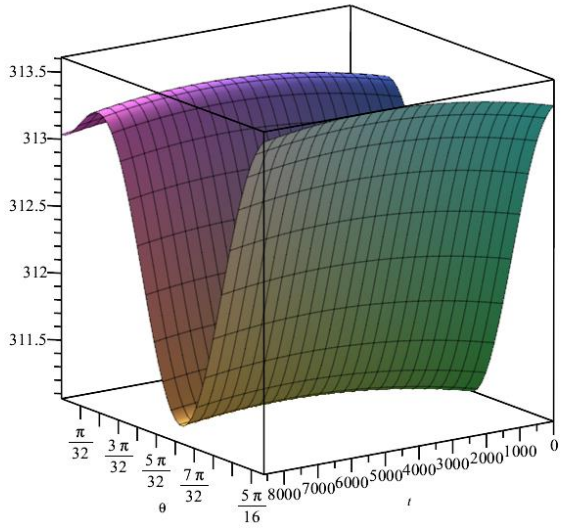

(a) Inner radius

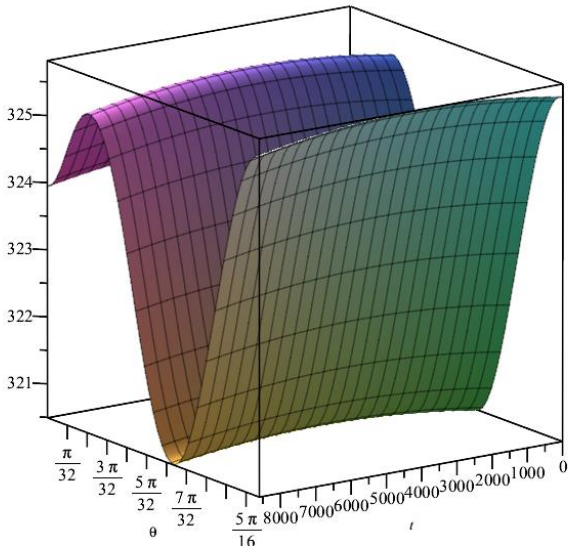

(b) Middle radius

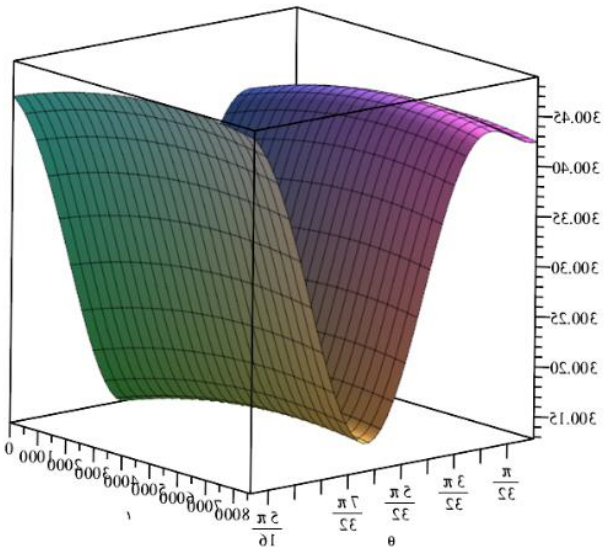

(c) Outer radius

Fig. 17 Three-dimensional temperature distribution in the curved beam with Boundary condition C

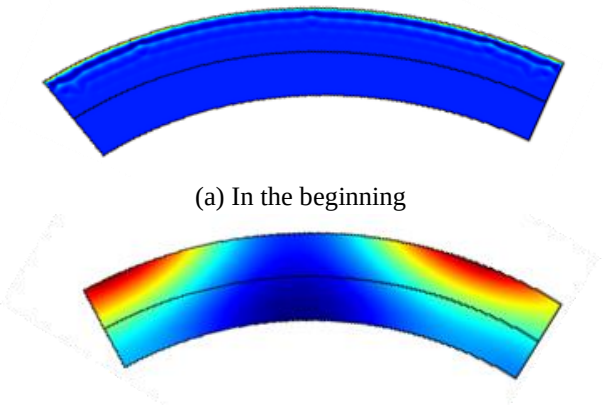

(a) In the beginning

(b) At the end

Fig. 18 Temperature change a curved beam modeled by COMSOL with Boundary condition C

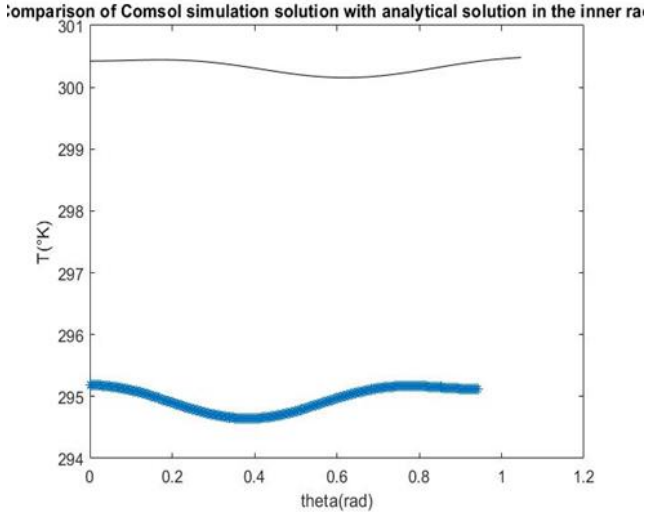

(a) Outre radius

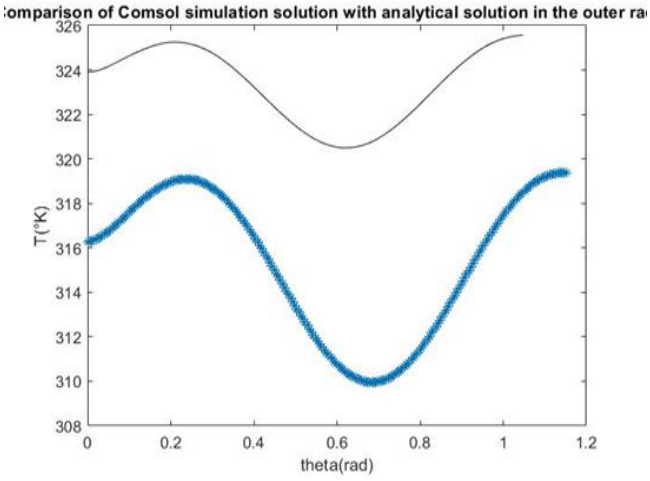

(b) Inner radius

Fig. 19 Comparison between analytical and those results obtained from Comsol simulation

comparison indicates that the overall trends align closely, demonstrating a reasonable convergence between the analytical and numerical (COMSOL) results.

4.3 Results and validation of boundary condition type C

4.3.1 Analytical solution Results

Under boundary condition type C, the outer radius of the curved beam is subjected to thermal flux, while the inner radius experiences convection with air. The remaining two sides of the curved beam are thermally insulated. Fig. 16 illustrates the distribution of the applied thermal flux along the angular direction (θ) on the outer radius. In this section, the results of the analytical solution for this boundary condition are presented and analyzed. The corresponding thermal flux is defined by the equation provided in Eq. (40)

$$f(\theta) = 600 * sin(8 * \theta + 12.3) + 1700 \quad (40)$$

Fig. 17 presents the three-dimensional temperature distribution in the curved beam, obtained from the analytical solution, for the outer radius (a), middle radius (b), and inner radius (c). These diagrams illustrate the transient thermal behavior of the curved beam as a function of time and angular position (θ) at different radial locations.

For boundary condition type C, the effect of convective heat transfer on the inner radius is clearly more pronounced compared to boundary condition type A, where the inner radius was insulated. This distinction highlights the significant influence of convection on the overall thermal behavior of the curved beam.

4.3.2 Validation

Fig. 18 presents the COMSOL simulation results for the curved beam under boundary condition type C, showing the temperature distribution at two distinct time points: the beginning (a) and the end (b) of the heat transfer process. The simulation illustrates the transient thermal behavior of the curved beam, where an initially uniform temperature distribution gradually transforms into a complex, non-uniform pattern. This transformation results from the combined effects of applied thermal flux, convection, and the beam's curvature. The results underscore the importance of boundary conditions and geometry in shaping the thermal performance of the system.

The results of confirmation and validation of the analytical solution and numerical solution by CMSOL, which shows the closeness of the analytical solution with the numerical solution for case C, are shown in Fig. 19.

5. Conclusions

This study presents a comprehensive investigation of the transient thermal analysis of curved beams under various boundary conditions. Analytical solutions were derived using the method of separation of variables, considering three boundary condition types: Type A, Type B, and Type C. The accuracy of these solutions was validated by comparing them with numerical simulations performed in COMSOL, demonstrating strong agreement across all cases.

For boundary condition type A, the results indicated that the applied heat flux on the outer radius generated periodic temperature distributions, with a clear thermal gradient developing from the inner to the outer radius over time. The system exhibited heat dissipation as it progressed toward thermal equilibrium.

Under boundary condition type B, the temperature profile displayed periodic sinusoidal variations along the angular direction at different radial positions. The outer radius experienced the highest temperature, while the inner radius exhibited smaller fluctuations. This pattern aligned with the non-uniform heat flux applied to the system.

In boundary condition type C, which involved convection at the inner radius and heat flux on the outer radius, the temperature distribution demonstrated a complex interaction between radial and circumferential heat transfer. A significant thermal gradient developed, influenced by the combined effects of convection and the applied thermal flux.

In all boundary conditions, temperature decreased over time as the system approached thermal equilibrium, with variations shaped by the beam's curvature and boundary conditions. The analytical solutions accurately captured both the periodicity and thermal gradients present in the curved beams.

This study underscores the importance of precise heat transfer modeling in curved structures, as thermal gradients and periodic temperature variations can significantly impact structural behavior. The findings validate the analytical solutions as reliable and efficient tools for analyzing transient thermal conditions, providing a solid foundation for future research on stress, strain, and vibrations in curved beams.

References

Abouelregal, A.E. and Alesemi, M. (2022), "Evaluation of the thermal and mechanical waves in anisotropic fiber-reinforced magnetic viscoelastic solid with temperature-dependent properties using the MGT thermoelastic model", *Case. Studies. Therm. Eng.*, **36**, 102187. https://doi.org/10.1016/j.csite.2022.102187.

Adab, N. and Arefi, M. (2022), "Vibrational behavior of truncated conical porous GPL-reinforced sandwich micro/nano-shells", *Eng. Comput.*, **39**(1), 419-443. https://doi.org/10.1007/s00366-021-01580-8.

Aljadani, M.H. and Zenkour, A.M. (2022), "A modified two-relaxation thermoelastic model for a thermal shock of rotating infinite medium", *Materials*, **15**, 9056. https://doi.org/10.3390/ma15249056.

Amiri Delouei, A., Emamian, A., Karimnejad, S., Sajjadi, H. and Jing, D. (2020), "Two-dimensional analytical solution for temperature distribution in FG hollow spheres: General thermal boundary conditions", *Int. Commun. Heat. Mass. Transf.*, **113**, 104531. https://doi.org/10.1016/j.icheatmasstransfer.2020.104531.

Andey, S. and Pradyumna, S. (2021), "Thermal shock analysis of functionally graded sandwich curved beams using a new layerwise theory", *Z. Angew. Math. Mech.*, **101**, e202100020. https://doi.org/10.1002/zamm.202100020.

Ansari, R., Oskouie, M.F., Nesarhosseini, S. and Rouhi, H. (2022), "Nonlinear thermally induced vibration analysis of porous FGM Timoshenko beams embedded in an elastic medium", *Transp. Por. Med.*, **142**, 63-87. https://doi.org/10.1007/s11242-021-01714-y.

Araya, G. and Gutierrez, G. (2006), "Analytical solution for a transient, three-dimensional temperature distribution due to a moving laser beam", *Int. J. Heat. Mass. Transf.*, **49**(19-20), 4124-

4131. https://doi.org/10.1016/j.ijheatmasstransfer.2006.03.026.
Arefi, M. and Zenkour, A.M. (2019), "Influence of magneto-electric environments on size-dependent bending results of three-layer piezomagnetic curved nanobeam based on sinusoidal shear deformation theory", *J. Sandw. Struct. Mater.*, **21**(8), 2751-2778. https://doi.org/10.1177/1099636217723186.
Arefi, M. and Civalek, O. (2020) "Static analysis of functionally graded composite shells on elastic foundations with nonlocal elasticity theory", *Arch. Civil. Mech. Eng.*, **20**(1), 1-17. https://doi.org/10.1007/s43452-020-00032-2
Arefi, M. (2018), "Nonlocal free vibration analysis of a doubly curved piezoelectric nano shell", *Steel. Compos. Struct.*, **27**(4), 479-493. https://doi.org/10.12989/scs.2018.27.4.479
Arefi, M. and Mohammad-Rezaei Bidgoli, E. (2019), "Electro-elastic displacement and stress analysis of the piezoelectric doubly curved shells resting on Winkler's foundation subjected to applied voltage", *Mech. Adv. Mater. Struct.*, **26**(23), 1981-1994. https://doi.org/10.1080/15376494.2018.1455937.
Arefi, M. and Kiani, M. (2020) "Magneto-electro-mechanical bending analysis of three-layered exponentially graded microplate with piezomagnetic face-sheets resting on Pasternak's foundation via MCST", *Mech. Adv. Mater. Struct.*, **27**(5), 383-395. https://doi.org/10.1080/15376494.2018.1473538
Arefi, M.M.R., Bidgoli, E. and Civalek, O. (2022), "Bending response of FG composite doubly curved nanoshells with thickness stretching via higher-order sinusoidal shear theory", *Mech. Based. Des. Struct. Mach.*, **50**(7), 2350-2378. https://doi.org/10.1080/15397734.2020.1777157
Azzara, R., Carrera, E., Filippi, M. and Pagani, A. (2023), "Vibration analysis of thermally loaded isotropic and composite beam and plate structures", *J. Therm. Stress.*, **46**(5), 369-386. https://doi.org/10.1080/01495739.2023.2188399.
Bai, B., Wu, H., Zhou, R., Wu, N. and Zhang, B. (2025a), "A granular thermodynamic framework-based coupled multiphase-substance flow model considering temperature driving effect", *J. Rock. Mech. Geotech. Eng.*, **17**(9), 5816-5828 https://doi.org/10.1016/j.jrmge.2024.11.017.
Bai, B., Wu, H., Wu, N. and Zhang, B. (2025b), "Granular thermo-dynamic ideology on the heavy metal migration in unsaturated soils driven by seepage-temperature", *J. Hydrol.*, **661**, 133738. https://doi.org/10.1016/j.jhydrol.2025.133738
Bai, B., Zhang, B., Ji, Y. and Zong, Y. (2025c), "A thermodynamic multi-field model for unsaturated sulfate-saline soils considering crystallization process", *Comput. Geotech.*, **184**, 107251. https://doi.org/10.1016/j.compgeo.2025.107251
Beg, M.S. and Yasin, M.Y. (2021), "Bending, free and forced vibration of functionally graded deep curved beams in thermal environment using an efficient layerwise theory", *Mech. Mater.*, **159**, 103919. https://doi.org/10.1016/j.mechmat.2021.103919.
Boğa, C. and Selek, O. (2020), "Stress analysis of functionally graded beams due to thermal loading", *Journal of Eng Sci and Tech*, 15(1), 54-65.
Boley, B.A. and Euval, S.B. (1958), "Thermal stress in curved beams", *J. Aer. Sci*, **25**(10), 627-630. https://doi.org/10.2514/8.7814
Boo, K.S. and Cho, H.S. (1990), "Transient temperature distribution in arc welding of finite thickness plates", *Proc. Inst. Mech. Eng., Part B: J. Eng. Manu.*, **204**(3), 175-184.
Chen, Y., Zhang, Y., Long, J., Xu, K. and Zhong, T. (2025c), "Multiscale cellulose-based optical management films with tunable transparency and haze fabricated by different bamboo components and mechanical defibrillation approaches", *Carbohydr. Polym.*, **348**, 122811. https://doi.org/10.1016/j.carbpol.2024.122811
Chen, Z., Pu, Q., Zhu, L. and Zhou, W. (2025a), "Creep behaviour between resilient wheels and rails in a metro system", *Vehicle Syst. Dyn.*, 1-21. https://doi.org/10.1080/00423114.2025.2494861.
Chen, Z., Zhou, W., Kuang, H., Chen, Z., Yang, J., Chen, Z. and Chen, F. (2025b), "Dynamic model and vibration of rack vehicle on curve line", *Vehicle Syst. Dyn.*, 1-19. https://doi.org/10.1080/00423114.2025.2494835
Civalek, Ö., Akbaş, Ş.D., Akgöz, B. and Dastjerdi, S. (2021), "Forced vibration analysis of composite beams reinforced by carbon nanotubes", *Nanomaterials*, **11**(3), 571, https://doi.org/10.3390/nano11030571
Civalek, O. and Demir, C. (2011), "Buckling and bending analyses of cantilever carbon nanotubes using the Euler-Bernoulli beam theory based on non-local continuum model", *Asian. J. Civ. Eng.*, **12**(5), 651-661, https://sid.ir/paper/299014/en
COMSOL Inc. (2013), http://www.comsol.com
Din, Q., Ishaque, W., Maqsood, I. and Tounsi, A. (2023), "Discretization of laser model with bifurcation analysis and chaos control", *Adv. Nano. Res.*, **15**(1), 25-34. https://doi.org/10.12989/anr.2023.15.1.025.
Eslami, M.R., Babaei, M.H. and Poultangari, R. (2005), "Thermal and mechanical stresses in a functionally graded thick sphere", *Int. J. Pres. Ves. Pip.*, **82**, 522-527. https://doi.org/10.1016/j.ijpvp.2005.01.002.
Feng, G., Jiang, F., Hu, Z., Jiang, W., Liu, J., Zhang, Q., Wu, Q., Hu, Q., Miao, L. and Cheng, S. (2020), "A novel porous egg-white (EW)/titania composite photocatalytic material for efficient photodegradation applications", *RSC. Adv.*, **14**. https://doi.org/doi.org/10.1039/d0ra00730g.
Hadji, L., Avcar, M. and Civalek, Ö. (2021), "An analytical solution for the free vibration of FG nanoplates", *J Brazil Soc. Mech. Sci. Eng.*, **43**, 418. https://doi.org/10.1007/s40430-021-03134-x
Haskul, M. (2019), "Thermal Stresses in a Cylindrically Curved FGM Beam", *Int. J. Eng. Res. Develop.*, **1**(1), 25-39.
Hetnarski, R.B. and Eslami, M.R. (2019), *Thermal Stresses—Advanced Theory and Applications*, Springer, Cham, Switzerland.
Jiang, H.J. and Dai, H.L. (2015), "Analytical solutions for three-dimensional steady and transient heat conduction problems of a double-layer plate with a local heat source", *Int. J. Heat. Mass. Transf.*, **89**, 652-666. https://doi.org/10.1016/j.ijheatmasstransfer.2015.05.094.
Jin, Z.H. and Paulino, G.H. (2001), "Transient thermal stress analysis of an edge crack in a functionally graded material", *Int. J. Fract.*, **107**, 73-98. https://doi.org/10.1023/A:1026583903046
Kadiri, A., Bendaida, M., Attia, A., Balubaid, M., Mahmoud, S. R., Bousahla, A.A., Tounsi, A., Bourada, F. and Tounsi, A. (2024), "Wave propagation in FG polymer composite nanoplates embedded in variable elastic medium", *Adv. Nano. Res.*, **17**(3), 235-248. https://doi.org/10.12989/anr.2024.17.3.235
Kumar, Y. Gupta, A. Tounsi, A. (2021) "Size-dependent vibration response of porous graded nanostructure with FEM and nonlocal continuum model", *Adv. Nano. Res.* **11**(1), 1-17. https://doi.org/10.12989/anr.2021.11.1.001
Liu, J., Ma, C., Li, M., He, J., Totis, G., Hua, C., ... and Weng, S. (2025a), "A compressed tensor-based edge-deployable framework for multi-source thermal error compensation in face gear machining", *Adv. Eng. Inform.*, **68**, C, 103802, https://doi.org/10.1016/j.aei.2025.103802
Liu, Y., Su, J., He, D., Hao, P., Liu, Y., Wang, Z. and Wang, T. (2025b), "Analytical model for corrugated rolling of composite plates considering the shear effect", *J. Manuf. Proc.*, **134**, 1069-1081. https://doi.org/10.1016/j.jmapro.2025.01.025
Luo, Y.X., Dong, Y.L., Yang, F.Q. and Lu, X.Y. (2024), "Ultraviolet single-camera stereo-digital image correlation for deformation measurement up to 2600 °C", *Exp. Mech.*, **64**(8), 1343-1355. https://doi.org/10.1007/s11340-024-01087-5
Ma, C., Huang, S. and Li, M. (2025a), "Highly efficient heat

dissipation method of grooved heat pipe for thermal behavior regulation for spindle system working in low rotational speed", *Int. Com. Heat. Mass. Transf.*, **169**, A, 109575. https://doi.org/10.1016/j.icheatmasstransfer.2025.109575

Ma, C., Li, M. and Liu, J. (2025b), "High-efficiency topology optimization method for thermal-fluid problems in cooling jacket of high-speed motorized spindle", *Int. Com. Heat. Mass. Transf.*, **169**, A, 109533. https://doi.org/10.1016/j.icheatmasstransfer.2025.109533

Malekzadeh, P., Golbahar Haghighi, M.R. and Atashi, M.M. (2010), "Out-of-plane free vibration of functionally graded circular curved beams in thermal environment", *Compos. Struct*, **92**(5), 541-552. https://doi.org/10.1016/j.compstruct.2009.08.040.

Malekzadeh, P., Heydarpour, Y. and Golbahar Haghighi, M.R. (2012), "Transient response of rotating laminated functionally graded cylindrical shells in thermal environment", *Int. J. Pres. Ves. Piping*. **98**, 43-56. https://doi.org/10.1016/j.ijpvp.2012.07.003.

Mohammadi, M. and Dryden, J.R. (2008), "Thermal stress in a nonhomogeneous curved beam", *J. Therm. Stress*, **31**(7), 587-598. https://doi.org/10.1080/01495730801978471.

Ootao, Y. and Ishihara, M. (2013), "Three-dimensional solution for transient thermoelastic problem of a functionally graded rectangular plate with piecewise exponential law", *Compos. Struct*., **106**, 672-680. https://doi.org/10.1016/j.compstruct.2013.06.019.

Qian, H., Qiu, Y.X., Lu, C.H. and Yang, Y. (2022), "Analytical solution of temperature in laminated beams subjected to general thermal boundary conditions", *J. Cent. South Univ*., **29**(2), 561-571. https://doi.org/10.1007/s11771-022-4911-2.

Quan, T.Q., Ha, D.T.T. and Duc, N.D. (2022), "Analytical solutions for nonlinear vibration of porous functionally graded sandwich plate subjected to blast loading", *Thin .Walled. Struct*, **170**, 108606. https://doi.org/10.1016/j.tws.2021.108606.

Sadooghi, P. (2005), "Transient heat transfer in a spherical protective material submitted to flux and mixed boundary conditions: an investigation on zirconia", *J. Quantit. Spectrosc. Rad. Transf.* **93**(5), 461-472. https://doi.org/10.1016/j.jqsrt.2004.07.037.

Sayyad, A.S. and Avhad, P.V. (2022), "Higher-order model for the thermal analysis of laminated composite, sandwich, and functionally graded curved beams", *J. Therm. Stresses*., **45**(5), 382-400. https://doi.org/10.1080/01495739.2022.2050476.

Shang, C., Nan, H., Bai, C., Zhang, L., Sun, G., Qiao, Y., Zheng, T. (2025), "The PEEK sizing agents modified by different dimensions nanomaterials of MXene and CNTs for enhancing the interfacial and mechanical properties of carbon fiber composites", *Colloids. Surf. A: Phys. Eng. Asp*., **726**, 137997. https://doi.org/10.1016/j.colsurfa.2025.137997

Sobhani, E., Masoodi, A.R., Civalek, O. and Ahmadi-Pari, A.R. "Agglomerated impact of CNT vs. GNP nanofillers on hybridization of polymer matrix for vibration of coupled hemispherical-conical-conical shells", *Aer. Sci. Tech.* **120**, 107257, 2022. https://doi.org/10.1016/j.ast.2021.107257

Su, G., Xiong, J. and Li, Q. (2023), "Gaseous formaldehyde adsorption by eco-friendly, porous bamboo carbon microfibers obtained by steam explosion, carbonization, and plasma activation", *Chem. Eng. J*., **455**, 140686. https://doi.org/10.1016/j.cej.2022.140686

Tahani, M., Talebian, T. and Todoroki, A. (2010), "Transient analysis of functionally graded thick hollow circular cylinders under mechanical loadings", *J. Solid. Mech. Mater. Eng*., **4**(8), 1223-1234. https://doi.org/10.1299/jmmp.4.1223.

Tang, H., Peng, J., Peng, H., Yang, Y., Gao, Q., Xiao, L., Yang, Z. (2025), "Test and theoretical investigations on flexural behavior of high-performance h-shaped steel beam with local corrosion in pure bending zone", *Steel. Res. Int*., **96**(7), 2400640. https://doi.org/10.1002/srin.202400640

Tang, X., Guo, C., Li, F., Zhang, R., Song, D., Fu, P. and Liu, H. (2023), "Thermal buckling analysis of rotationally-restrained orthotropic thin plates utilizing a two-dimensional improved Fourier series approach", *Meccanica*, **58**, 1443-1464. https://doi.org/10.1007/s11012-023-01664-3.

Tlidji, Y., Benferhat, R., Daouadji, T.H., Tounsi, A. and Cong Trinh, L. (2022), "Free vibration analysis of FGP nanobeams with classical and non-classical boundary conditions using State-space approach", *Adv. Nano. Res.* **13**(5), 453-463. https://doi.org/10.12989/anr.2022.13.5.453.

Uzun, B., Civalek, Ö. and Yaylı, M.Ö. (2020), "Vibration of FG nano-sized beams embedded in Winkler elastic foundation and with various boundary conditions", *Mech. Based. Des. Struct. Mach*., **51**(1), 481-500. https://doi.org/10.1080/15397734.2020.1846560

Vali, H. and Arefi, M. (2023), "Extension of a novel higher order modeling to the vibration responses of sandwich graphene origami cylindrical panel", *Arch. Civ. Mech. Eng*., **23**, 268. https://doi.org/10.1007/s43452-023-00797-2

Wang, L., Wang, Z., Zhang, S., Tan, J., Lin, Y. and Xiang, Y. (2025a), "Multi-unit global-local registration for 3D bent tube based on implicit structural feature compatibility", *Adv. Eng. Inform*., **65**, 103120. https://doi.org/10.1016/j.aei.2025.103120

Wang, Z., Li, J., Yuan, Y., Zhang, S., Hu, W., Ma, J. and Tan, J. (2025b), "Digital-twin-enabled online wrinkling monitoring of metal tube bending manufacturing: A multi-fidelity approach using forward-convolution-GAN", *Appl. Soft. Comput*., **171**, 112684. https://doi.org/10.1016/j.asoc.2024.112684

Wu, M., Liu, Z., Qin, Y., Su, K. and Yu, Z. (2025), "Thermal property of reservoir rocks at thermal-mechanical coupled conditions and resultant impact on performance of geothermal systems", *Rock. Mech. Rock. Eng.*, **58**, 8773-8798. https://doi.org/10.1007/s00603-025-04587-5

Wu, X., Shi, J.Y., Lei, H., Li, Y.P. and Okine, L. (2019), "Analytical solutions of transient heat conduction in multilayered slabs and application to thermal analysis of landfills", *J. Cent. South Univ*., **26**(11), 3175-3187. https://doi.org/10.1007/s11771-019-4244-y.

Xiong, J., Hu, Q. and Wu, J. (2023), "Structurally stable electrospun nanofibrous cellulose acetate/chitosan biocomposite membranes for the removal of chromium ions from the polluted water", *Adv. Compos. Hybrid Mater*., **6**, 99. https://doi.org/10.1007/s42114-023-00680-x

Xiong, J., Wang, Y. and Wang, H. (2024), "Electrospun biomass carbon-based porous nanofibers modified by green-dry cold plasma for gaseous formaldehyde adsorption", *Ind. Crops. Prod*., **222**, 119769. https://doi.org/10.1016/j.indcrop.2024.119769

Xu, K., Liu, C., Kang, K., Zheng, Z. and Wang. S. (2018), "Isolation of nanocrystalline cellulose from rice straw and preparation of its biocomposites with chitosan: Physicochemical characterization and evaluation of interfacial compatibility", *Compos. Sci. Tech*., **154**, 8-17. https://doi.org/10.1016/j.compscitech.2017.10.022

Yang, J., Huang, X.H. and Shen, H.S. (2020), "Nonlinear vibration of temperature-dependent FG-CNTRC laminated beams with negative Poisson's ratio", *Int. J. Struct. Stabil. Dyn*., **20**(4), 2050043. https://doi.org/10.1142/S0219455420500431.

Yang, Y., Dai, H.L., Ye, C., Xu, W.L. and Luo, A.H. (2019), "Investigation of the one-dimensional transient heat conduction problem of a coated high strength steel plate", *Math. Mech. Solid*., **24**(11), 3472-3484. https://doi.org/10.1177/1081286519847709.

Yang, Z. and Zhu, H. (2023), "Study on the effect of carbon nanotubes on the microstructure and anti-carbonation properties

of cement-based materials", *J. Func. Mater.*, **54**(8), 8217-8227. https://doi.org/10.3969/j.issn.1001-9731.2023.08.027.

Yang, N. and Zou, Y. and Arefi, M. (2023a), "Bending results of graphene origami reinforced doubly curved shell", *Def. Tech.*, **35**, 198-210. https://doi.org/10.1016/j.dt.2023.11.017.

Yapıcı, H. and Baştürk, G. (2005), "Numerical solutions of transient temperature and thermally induced stress distributions in a solid disk heated with radially periodic expanding and contracting ring heat flux", *J. Mater. Prod. Tech.*, **159**(1), 99-112. https://doi.org/10.1016/j.jmatprotec.2004.04.412

Yapıcı, H., Genç, M.S. and Özışık, G. (2008), "Transient temperature and thermal stress distributions in a hollow disk subjected to a moving uniform heat source", *J. Therm. Stress.*, **31**(5), 476-493. https://doi.org/10.1080/01495730801912652.

Yousefi, A. and Rastgoo, A. (2011), "Free vibration of functionally graded spatial curved beams", *Compos. Struct.*, **93**(4), 3048-3056. https://doi.org/10.1016/j.compstruct.2011.04.024.

Zhang, H., Shi, Y., Fan, Z. and Chen, R. (2012), "Marching-on-in-degree solver of time domain finite element-boundary integral method", *Asia. Pac. Microwave. Conf. Proc.*, Kaohsiung, Taiwan, 340-342. https://doi.org/10.1109/APMC.2012.6421591.

Zhang, S., Yang, Y. and Yang, H. (2017), "A meshless symplectic algorithm for nonlinear wave equation using highly accurate RBFs quasi-interpolation", *Appl. Math. Comput.* **314**(1), 110-120. https://doi.org/10.1016/j.amc.2017.07.010.

Zhang, M., Jiang, X. and Arefi, M. (2023a), "Dynamic formulation of a sandwich microshell considering modified couple stress and thickness-stretching", *Eur. Phys. J. Plus.*, **138**(3), 227. https://doi.org/10.1140/epjp/s13360-023-03753-4.

Zhang, Z., Sun, Y., Xiang, Z., Qian, W. and Shao, X. (2023b), "Transient thermoelastic analysis of rectangular plates with time-dependent convection and radiation boundaries", *Buildings*, **13**, 2174. https://doi.org/10.3390/buildings13092174.

Zhang, K., Zhu, C. and Xie, Z. (2025), "Facile fabrication of electrospun hybrid nanofibers integrated cellulose, chitosan with ZIF-8 for efficient remediation of copper ions", *Carbohyd. Polym.*, **359**, 123574. https://doi.org/10.1016/j.carbpol.2025.123574

Zhou, Y., Xia, Y., Chen, B. and Fujino, Y. (2020), "Analytical solution to temperature-induced deformation of suspension bridges", *Mech. Syst. Signal. Pr.*, **139**, 106568. https://doi.org/10.1016/j.ymssp.2019.106568.

Zou, D., Liu, G., Rao, Z., Tan, T., Zhang, W. and Liao, W. (2021), "A device capable of customizing nonlinear forces for vibration energy harvesting, vibration isolation, and nonlinear energy sink", *Mech. Syst. Signal. Proc.*, **147**, 107101. https://doi.org/10.1016/j.ymssp.2020.107101

CC